

# Project 1: Density Functional Theory Structural Stability and Heat of Formation

CANDIDATE NUMBER: 1024785

University of Oxford, January 2020

1490 words

## I. INTRODUCTION

This project uses Density Functional Theory (DFT) to examine several material systems and their properties. Specifically, the structural stability of Si, Al, Ti, AlSi, and TiAl; the density of states of Si, Ti and Al; and the heat of formation of compounds AlSi and TiAl. The heat of formation indicates whether a structure would prefer to be in separate elemental phases, or exist as an alloy.

DFT is a computational modelling method built from quantum mechanical first principles. It works on the electronic scale, and can be used to deduce the electronic structure of materials to determine their ground state properties such as: band-structure, lattice constant, and charge densities.

The Schrödinger equation for a many-body system is

$$\hat{H}\psi(\mathbf{r}_1, \mathbf{r}_2, \dots, \mathbf{r}_N) = E\psi(\mathbf{r}_1, \mathbf{r}_2, \dots, \mathbf{r}_N) \quad (1)$$

where  $N$  is the total number of electrons, and  $E$  is the total energy of the system. DFT provides a way to avoid having to solve this complex equation by using the Hohenberg-Kohn theorem. This theorem describes the energy as a unique functional of the electron density.

$$E = E[\rho(\mathbf{r})] \quad (2)$$

Kohn and Sham split the energy functional into two separate terms (Hartree and exchange-correlation energy) to give

$$\hat{H}\psi_i(\mathbf{r}) = \left( -\frac{1}{2}\nabla^2 + V_{\text{ion}} + V_{\text{H}} + V_{\text{xc}} \right) = \epsilon_i\psi_i(\mathbf{r}) \quad (3)$$

This allows the many-body problem to be translated into an effective one-electron problem. By using the local density approximation (LDA), which treats the local electron density as that of a uniform electron gas at each point,  $V_{\text{H}}$  and  $V_{\text{xc}}$  depend explicitly on the total electronic density, and so can be calculated<sup>[1]</sup>.

This project uses CASTEP code which works under the above approximations to find self-consistent solutions. The method used (the plane-wave basis) uses a set of basis functions to represent the wave function. It is a simple and unbiased approach which satisfies Bloch's theorem, avoiding the need to perform multiple calculations over many atoms. Pseudopotentials are used to describe the wavefunctions near the

atom cores; calculations can be further simplified under this assumption that repulsive electron interactions are largely cancelled out by the attractive Coulomb potential inside the ion cores.

The density is determined by using a uniform mesh of  $k$ -points in  $k$ -space. To avoid summing over infinite  $k$ -points in the plane-wave expansion, it is necessary to choose a  $k$ -value cut-off corresponding to when the energy converges. Figure 1 below illustrates how self-consistent results are obtained by CASTEP.

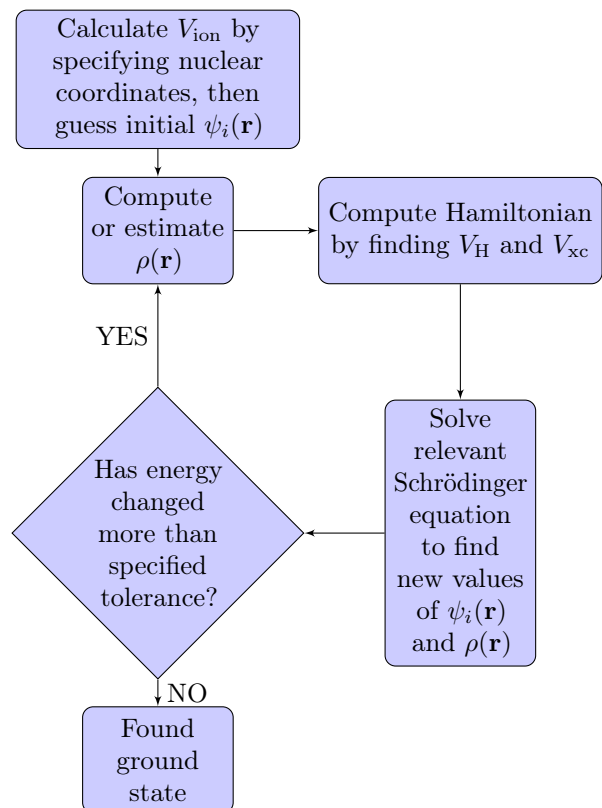


**Figure 1:** Method used by CASTEP to find a self-consistent solution

## II. RESULTS AND DISCUSSION

### i. Convergence of DFT Calculations: Si

To ensure the accuracy of DFT calculations, convergence tests of the CASTEP simulations are performed with respect to energy cutoff and  $k$ -points. In this project, convergence of the lattice constant was defined as: the value at which deviation from the previous calculation was no more than  $\pm 0.01\text{\AA}$ .

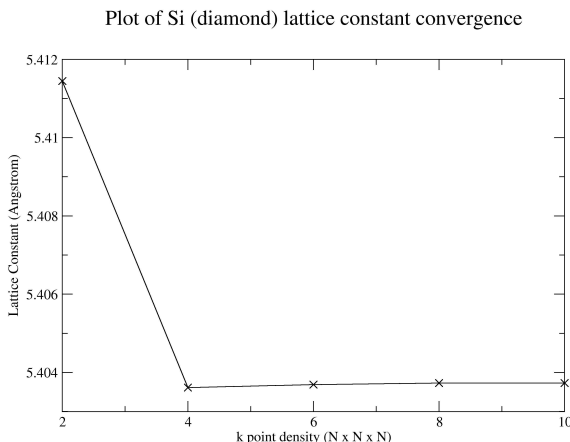


**Figure 2:** Lattice constant vs  $k$ -point density

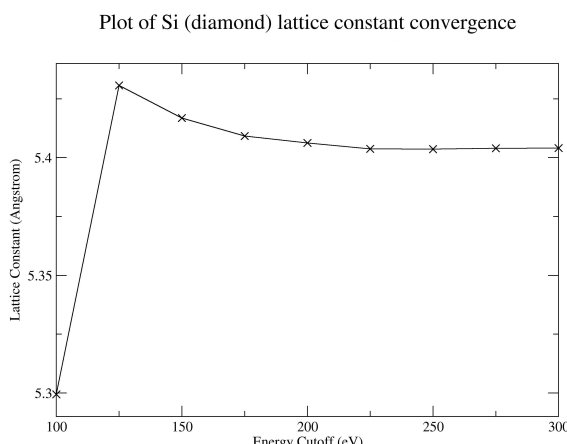


**Figure 3:** Lattice constant vs energy cutoff

As shown in figures 2 and 3, the  $k$ -point and energy cutoff calculations converged at  $5.404\text{\AA}$  for values of  $6 \times 6 \times 6$  and 250eV. The literature value of  $5.431\text{\AA}$ <sup>2</sup> compares well with the results (0.5% larger). This difference between the two quantities is likely to be accounted for by thermal expansion (the literature uses  $T = 300\text{K}$ , whilst DFT calculations assume  $T = 0\text{K}$ ).

### ii. Structural Stability of Si

DFT was used for four cubic structures to find the most stable configuration. The structures were: BCC (body centred cubic), FCC (face centred cubic), SC (simple cubic), and diamond. A Murnaghan fit was used. As shown in figure 4, the most thermodynamically stable structure of silicon is diamond, which has the lowest energy per atom of  $-169.0\text{eV}$ .

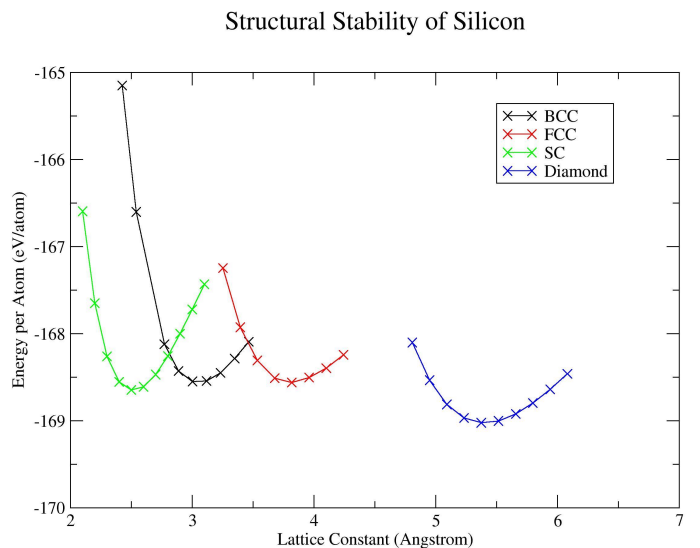


**Figure 4:** Energy of different silicon structures

### iii. Density of States of Si

The density of states of silicon and aluminium were calculated using DFT, and are plotted in figures 5 and 6 respectively. From the results it is found that  $\varepsilon_F, \text{Al} = 5.27\text{eV}$ , and  $\varepsilon_F, \text{Si} = 17.72\text{eV}$ , where  $\varepsilon_F$  is the Fermi Energy. Both graphs follow the  $y = \sqrt{x}$  trend expected from the model of a 3D free electron gas (FEG). Aluminium has a smoother curve, showing that it fits the FEG model better than silicon. The deviation from the FEG model seen in silicon is likely explained by the presence of the extra valence electron. This enters the partially-filled 3p orbital, and interacts with the other 3p electron.  $\varepsilon_F$  does not fall within the band gap for either graphs, so it is expected that metallic behaviour is observed. In practice, this is true for aluminium, whilst silicon has a diamond structure and acts as a semiconductor (its  $\varepsilon_F$  actually falls in a band gap: highlighting one of the limitations of DFT further discussed in section III).

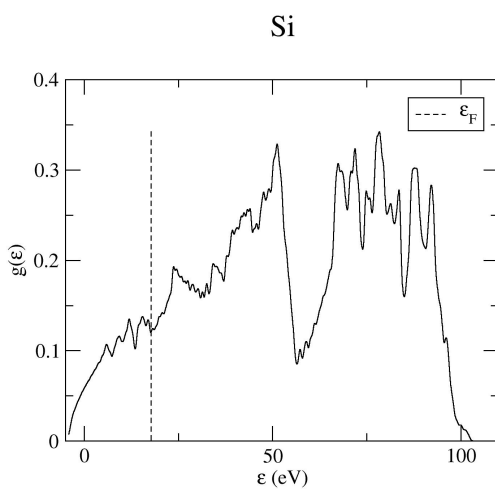


**Figure 5:** Density of States of Si(FCC): Gaussian-broadening=0.8.

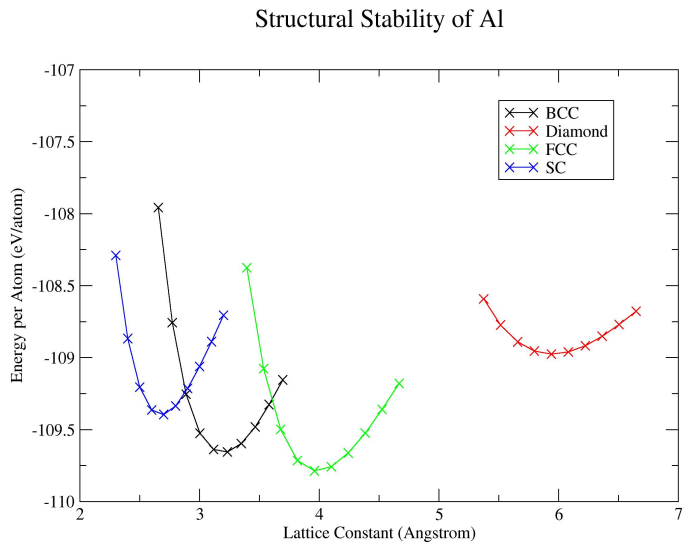


**Figure 7:** Energy of different aluminium structures

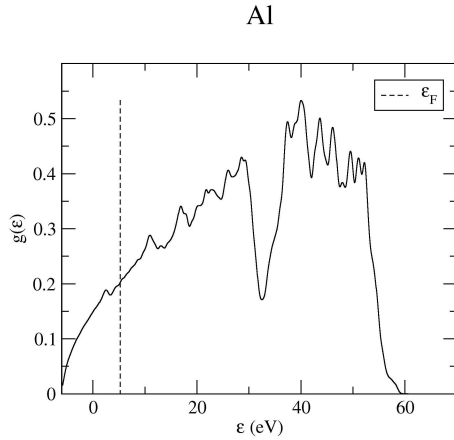


**Figure 6:** Density of States of Al(FCC): Gaussian-broadening=0.8.

#### iv. Structural Stability of Al

Given previous findings in section [i](#) and the relative similarity of aluminium to silicon, it was deemed sufficient to use the  $k$ -point density of  $10 \times 10 \times 10$  for aluminium calculations. The most thermodynamically stable structure is found to be FCC, as shown in figure [7](#). The lattice parameter of this state is  $3.96\text{\AA}$ , with energy per atom of  $-109.8\text{eV}$ . The literature value is  $4.05\text{\AA}$ <sup>2</sup>, showing a difference of 2%. Again, the DFT value is probably smaller because the model uses  $T = 0\text{K}$ . Aluminium has a larger thermal coefficient than silicon ( $23.6 \times 10^{-6} \text{ }^{\circ}\text{C}^{-1}$  and  $2.6 \times 10^{-6} \text{ }^{\circ}\text{C}^{-1}$  respectively)<sup>3</sup>, which explains the higher discrepancy between theoretical and experimental values.

#### v. Convergence of DFT Calculations: Ti

Convergence tests were run for titanium to the same criteria as in section [i](#). It has a more complex electronic structure because the partially filled d-orbital leads to more strongly localised wavefunctions. Therefore, it is expected that  $k$ -point density would need to be increased, and a larger basis set required. A lattice parameter of  $3.17\text{\AA}$  for  $k$ -point density  $12 \times 12 \times 12$ , and cut-off energy  $450\text{eV}$  was found, as shown in figures [8](#) and [9](#).

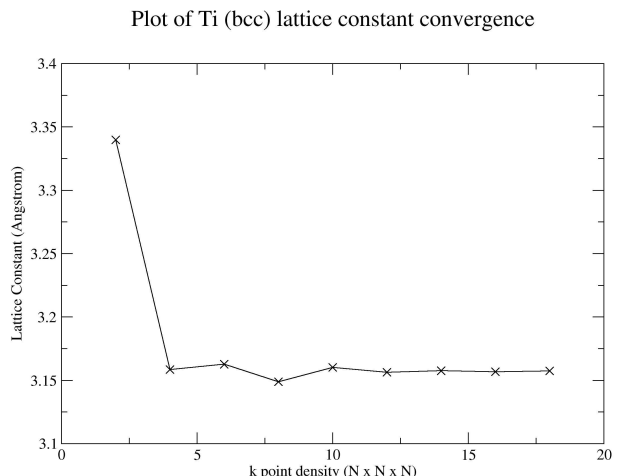


**Figure 8:** Lattice constant vs  $k$ -point density

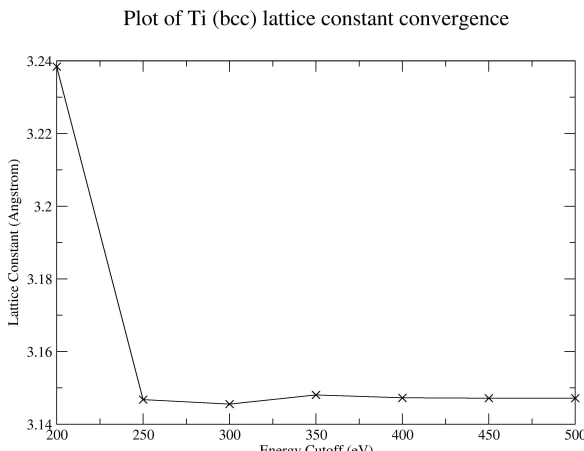


**Figure 9:** Lattice constant vs energy cutoff

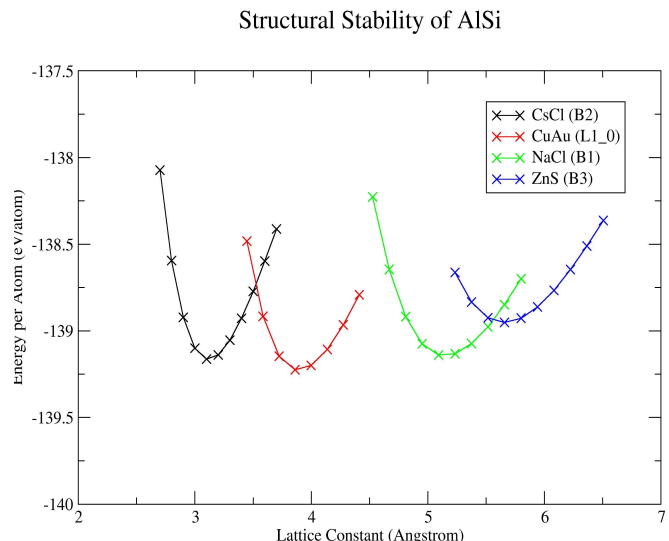


**Figure 11:** Energy of different AlSi structures

## vi. Structural Stability of Ti

The DFT simulation for titanium indicates that FCC is the most thermodynamically stable structure, with a lattice constant of 3.96 Å, and energy per atom of  $-1593.6\text{eV}$ , as shown in figure 10. In reality, the most stable structure is HCP (hexagonal close packed), but this was not included in the simulation.

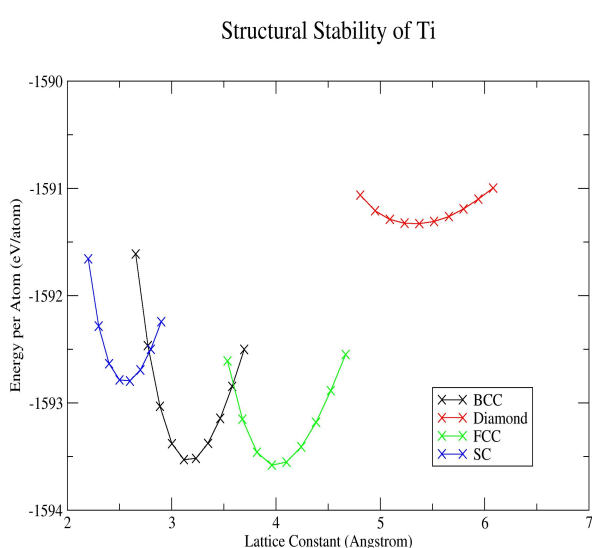


**Figure 10:** Energy of different titanium structures

## vii. Structural Stability and Heat of Formation: AlSi

The use of DFT was extended to find the most stable structure for compounds. The structures which were investigated were: B1 (NaCl), B2 (CsCl), B3 (ZnS), and L1<sub>0</sub> (CuAu).

For AlSi, figure 11 shows that L1<sub>0</sub> is the most thermodynamically stable structure with average energy per atom  $-139.2\text{eV}$ .

The following equation was used to determine the heat of formation of the compound.

$$\Delta H(\text{AlSi}) = E_{\text{tot}}(\text{AlSi}^{L1_0}) - \frac{1}{2}[E_{\text{tot}}(\text{Si}^{\text{diamond}}) + E_{\text{tot}}(\text{Al}^{\text{FCC}})] \quad (4)$$

Previous calculations were used to get:  $E_{\text{tot}}(\text{AlSi}^{L1_0}) = -139.2\text{eV atom}^{-1}$ ,  $E_{\text{tot}}(\text{Si}^{\text{diamond}}) = -169.0\text{eV atom}^{-1}$ , and  $E_{\text{tot}}(\text{Al}^{\text{FCC}}) = -109.8\text{eV atom}^{-1}$ . This gives

$$\Delta H(\text{AlSi}) = +0.20\text{eV atom}^{-1} = +19.26\text{kJ mol}^{-1}. \quad (5)$$

A positive value of  $\Delta H$  indicates that the compound is not stable, and is unlikely to exist. However, AlSi compounds are known to exist; when they have been stabilised with additional elements such as copper, magnesium, and manganese.<sup>4</sup>

## viii. Structural Stability and Heat of Formation: TiAl

L1<sub>0</sub> is found to be the most stable structure for TiAl, with average energy per atom  $-852.1\text{eV}$ . This is shown in figure 12.

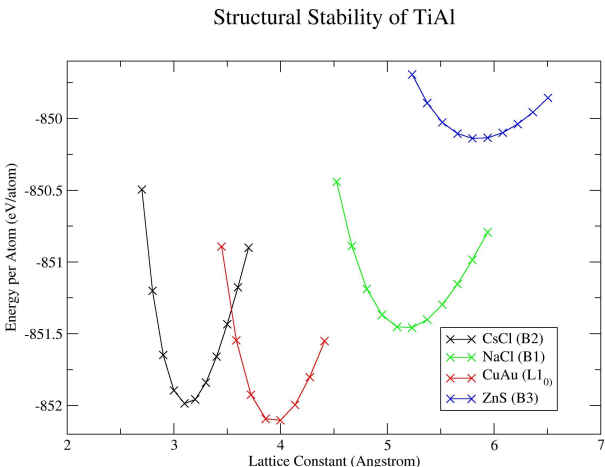


**Figure 12:** Energy of different TiAl structures

The heat of formation was calculated using

$$\Delta H(\text{TiAl}) = E_{\text{tot}}(\text{TiAl}^{L1_0}) - \frac{1}{2}[E_{\text{tot}}(\text{Ti}^{\text{BCC}}) + E_{\text{tot}}(\text{Al}^{\text{FCC}})] \quad (6)$$

Previous calculations were used to get:  
 $E_{\text{tot}}(\text{TiAl}^{L1_0}) = -852.1 \text{ eV atom}^{-1}$ ,  $E_{\text{tot}}(\text{Ti}^{\text{BCC}}) = -1593.6 \text{ eV atom}^{-1}$ , and  $E_{\text{tot}}(\text{Al}^{\text{FCC}}) = -109.8 \text{ eV atom}^{-1}$ . This gives

$$\Delta H(\text{TiAl}) = -0.40 \text{ eV atom}^{-1} = -38.6 \text{ kJ mol}^{-1}.$$

A negative heat of formation indicates that a stable TiAl compound probably exists, although this calculation uses FCC titanium, rather than its more stable HCP phase. In fact, TiAl alloys are used in the aerospace industry for high temperature applications such as turbine blades.<sup>5</sup>

### III. OUTLOOK

DFT has its limitations. It is known to underestimate band gap energies due to its use of the LDA. It also works badly for materials where van der Waals forces are predominant, such as graphite, because spontaneous dipole fluctuations are not considered in the model. Highly-correlated electron systems are also predicted poorly, because of the effective one-electron nature of the Kohn-Sham equations. Therefore, DFT cannot explain the entanglement of spins, a key aspect of quantum computing.

It is hard to model systems larger than 1000 atoms because of the computing power that would be needed, so DFT is often combined with other methods. For example, it is used to calculate properties such as bulk and elastic modulus which are useful in finite element methods (FEM). Another example would be to calculate diffusion rates for use in kMC models of catalytic reactions. These examples show the multi-scale use of DFT.

### IV. SUMMARY AND CONCLUSION

This project used DFT to find the most stable cubic structures of: silicon (diamond), aluminium (FCC), titanium (FCC), AlSi ( $L1_0$ ), and TiAl ( $L1_0$ ). In addition, the density of states of silicon and aluminium were compared. The additional valence electron in silicon results in a higher Fermi energy ( $\varepsilon_F$ , Al = 5.27eV, and  $\varepsilon_F$ , Si = 17.72eV) and worse fit of the FEG model. The heat of formation of AlSi (+19.26kJmol<sup>-1</sup>) and TiAl (-38.6kJmol<sup>-1</sup>) suggest that AlSi would be more stable in separate elemental phases, whilst TiAl could be found as an alloy. These DFT calculations exhibit a high degree of accuracy and compatibility with literature. In future investigation, it would be useful to include more complex crystal structures, such as HCP.

### REFERENCES

- <sup>1</sup> Giustino, F. *Materials Modelling using Density Functional Theory: Properties and Predictions* Oxford University Press, 2014.
- <sup>2</sup> Wolfram Research, Inc. *Lattice Constants of the Elements*. [Online]. Available at <https://periodictable.com/Properties/A/Lattice-Constants.html>. [Accessed 02/02/2020]
- <sup>3</sup> American Society for Metals International. *Thermal Properties of Metals*. [Online]. Available at <http://www.owlnet.rice.edu/msci301/Thermal-Expansion.pdf>. [Accessed 02/02/2020]
- <sup>4</sup> Cornell, R. et al. *Aluminium-Silicon Casting Alloys* [Online]. Available at <https://www.phase-trans.msm.cam.ac.uk/abstracts/M7-8.html>. [Accessed 02/02/2020]
- <sup>5</sup> Bewlay, B. et al. *TiAl alloys in commercial aircraft engines*. Materials at High Temperatures, Volume 33, Number 4-5, 2016., p. 549.

# Project 3: Kinetic Monte Carlo

## A Simple Model of a Catalytic Reaction

CANDIDATE NUMBER: 1024785

University of Oxford, January 2020

1492 words

### I. INTRODUCTION

In this project the kinetic Monte Carlo (kMC) model is used to model a simple catalytic surface reaction and to investigate its different parameters. These were the variation of rate and diffusion coefficient with: time taken between measurements, temperature, reaction concentration, and energy barriers to diffusion of reactants.

The kMC method creates a dynamic model of a system evolving between states by the generation of random numbers. It addresses the time-scale problem that finer grain models such as Molecular Dynamics (MD) have by ignoring the vibrational period of each atom, and instead focussing directly on state-to-state transitions. Therefore, kMC reaches time-scales of seconds. The model makes two key assumptions in order to coarse grain individual atomic degrees of freedom into a broader description of states. These assumptions simplify the model from an adatom which follows equations of motion to an adatom that hops from one lattice site  $i$  to a neighbouring site  $j$  with a rate  $\Gamma_{ij}$ . These are:

1. each adatom occupies a discrete lattice site, which is modelled as a potential well.
2. jumps between wells are instantaneous.

The above assumptions are reasonable to make: atoms are most stable in their lattice sites and are found there the majority of time. The probability of a specific event occurring is given by

$$\delta p_{i \rightarrow j} = \Gamma_{ij} \delta t. \quad (1)$$

In this specific model, a square lattice (made of catalytic material) has sites for two species ( $A$  and  $B$ ) from a gas phase to adsorb onto the surface. This is visualised in figure 1. Upon overcoming the activation energy barrier, reactant atoms diffuse across the surface via thermally activated jumps. A reaction occurs when  $A$  and  $B$  occupy the same adsorption site. However, this kMC model does not account for the kinetics associated with re-adsorption and de-adsorption of the particles.

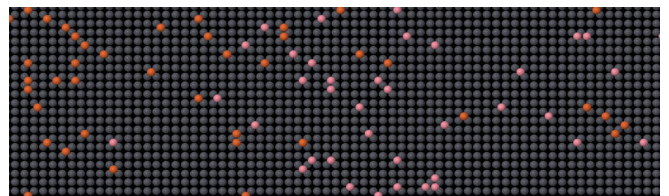


**Figure 1:** Visualisation of a catalytic crystal lattice with atoms  $A$  and  $B$  adsorbed onto the surface

Parameters which are input into the kinetic Monte Carlo method are often obtained from finer grain methods such as Density Functional Theory (DFT) or Molecular Dynamics (MD). These parameters include: initial occupation, defining each state, and rate constants for possible events. Figure 2 shows how this method is implemented on a computer<sup>[1]</sup>.

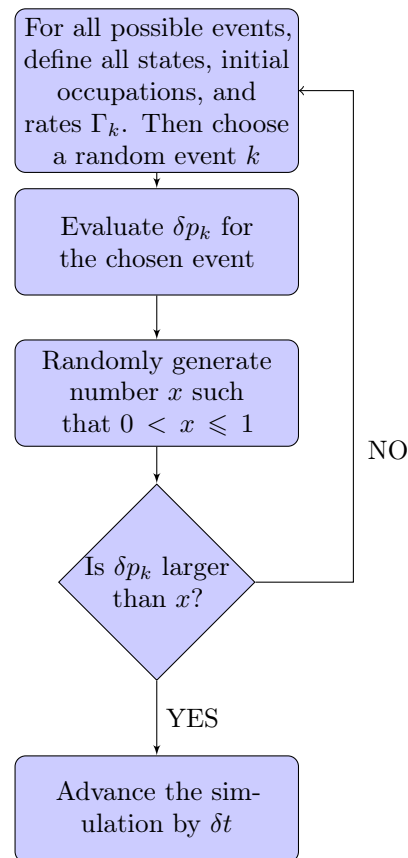


**Figure 2:** The implementation of kMC for a single event

## II. RESULTS AND DISCUSSION

All units in this project are arbitrary, as generic  $A$  and  $B$  atoms were used in the simulations, and  $\delta t$  (from equation 1) was set with a unit value.

### i. Mean Square Displacement (MSD) as a function of time

Figure 3 shows that  $MSD_A$ , the mean square displacement of a single atom  $A$ , is independent of the time between measurements,  $\Delta t$ . This is as expected because in this scenario,  $MSD_A$  is equal to  $D_A$ , the diffusion coefficient of  $A$ .  $D_A$  is a material property and is not affected by  $\Delta t$ . There is an increasing deviation from linear behaviour as  $\Delta t$  increases, because fewer measurements are being taken, so random deviation has a larger effect as the data is of poor statistical quality.

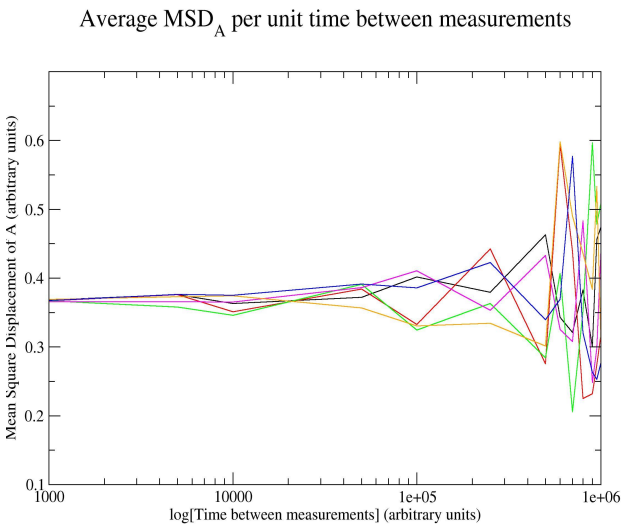


**Figure 3:** Different coloured lines represent different runs of the same simulation. Each instance a value of  $MSD_A$  was calculated, a random number was generated as the seed.

From figure 3, the average  $MSD_A$  value for the first four points was found to be  $0.37 \pm 0.03$  using standard deviation for error.

### ii. Mean Square Displacement as a function of temperature

From literature<sup>2</sup>, it is expected that the relationship between  $MSD_A$  and temperature is

$$MSD_A = \nu e^{-\frac{E_d}{k_B T}}. \quad (2)$$

where  $E_d$  is the energy of diffusion,  $T$  is temperature, and  $\nu$  is effective jump frequency. Equation 2 gives an

Arrhenius relationship

$$\ln(MSD_A) = \ln(\nu) - \frac{E_d}{k_B T} \quad (3)$$

which is plotted in figure 4

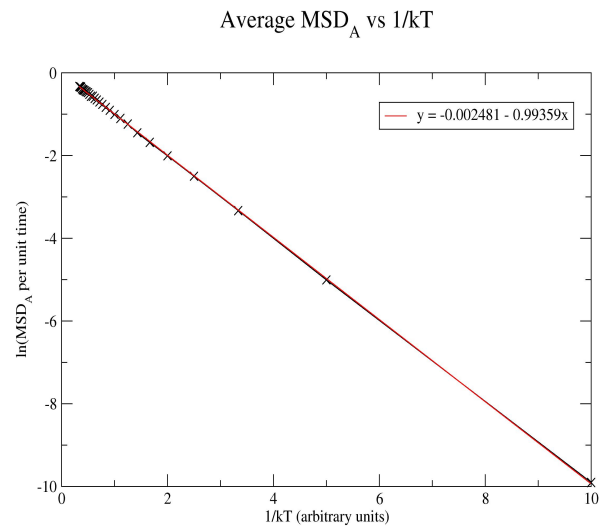


**Figure 4:**  $MSD$  as a function of  $T$  to calculate activation energy and attempt frequency for diffusion

This linear relationship is shown in figure 4, where the gradient is  $-E_d$ , and the y-intercept is  $\ln(\nu)$ .

$$E_d = 0.994, \ln(\nu) = 0.998. \quad (4)$$

This gives

$$MSD_A = 0.998 e^{-\frac{0.994}{k_B T}}. \quad (5)$$

This is expected as the input value of  $E_d$  and  $\ln(\nu)$  are both 1.

### iii. Concentration dependence of the reaction rate I

The fraction of sites occupied by  $A$  and  $B$  were varied to investigate the nature of the reaction. By increasing the concentration of each reactant, the number of collisions should linearly increase. Therefore, increasing both concentrations at the same time produces a quadratic fit. Figure 5 shows that simultaneously varying  $c_A$  and  $c_B$  fits a quadratic relationship well, where  $c_A$  and  $c_B$  are the fraction of sites occupied by  $A$  and  $B$  atoms respectively. The other graph plotted on figure 5 shows a linear relationship when only  $c_B$  was varied, as expected. This confirms an overall 2<sup>nd</sup> order rate of reaction. For low surface concentrations, the fit breaks down because there are too few atoms for reliable statistical analysis.

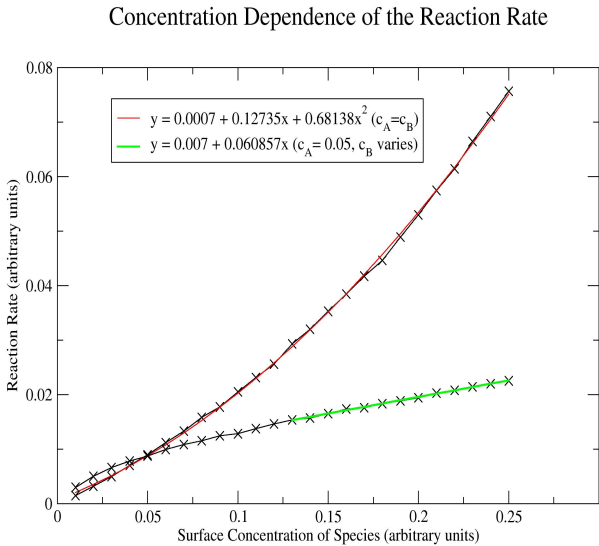


**Figure 5:** Concentration dependence of the reaction rate

#### iv. Temperature dependence of the reaction rate I

It is assumed by the catalyst model that a reaction between  $A$  and  $B$  will occur whenever the atoms occupy the same adsorption site. It follows that a reaction will happen if the temperature is high enough for diffusion to occur. Therefore, this type of surface reaction is considered ‘diffusion limited’. Therefore  $E_a$ , the overall activation energy, should be equivalent to  $E_d$  found in section ii. This explains why figure 6 shows a linear Arrhenius plot, similar to figure 4.

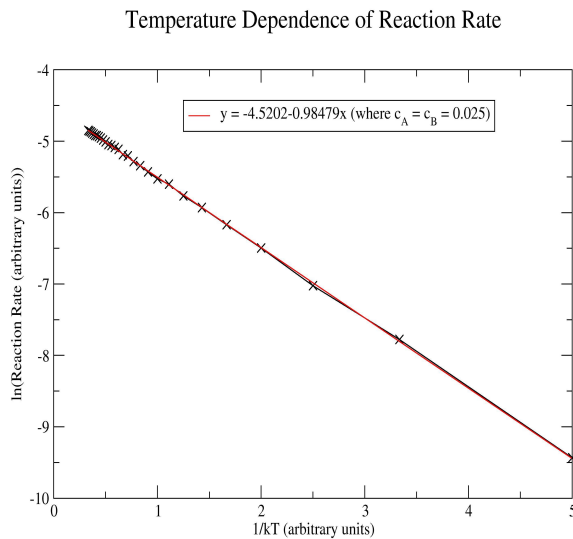


**Figure 6:** Temperature dependence of the reaction rate to calculate activation energy when total surface coverage from  $A$  and  $B$  atoms is 5%

From figure 6,  $E_a = 0.985$ . Given that  $E_d = 0.994$ , this confirms that  $E_a = E_d$ , since the 0.9% difference

is more than accounted for by experimental error. The y-intercept of figure 6 gives the Arrhenius prefactor:  $e^{-4.5202} = 0.011$ .

The overall T dependence of the rate is:

$$\text{rate}(T) = 0.011e^{-\frac{0.98}{k_B T}} \quad (6)$$

#### v. Coarse grained continuum model of the reaction rate

The calculated temperature and concentration dependencies can be combined into a single formula to describe the reaction rate on the catalytic surface.

Temperature dependency (from section iv) is

$$\text{rate}(T) = 0.011e^{-\frac{0.98}{k_B T}}. \quad (7)$$

Concentration dependency (from section iii) is

$$\text{rate} = 0.681[A]^1[B]^1 \quad (8)$$

where  $[A] = c_A$ , concentration of species  $A$ ,  $[B] = c_B$ , concentration of species  $B$ . Combining the two equations which contribute to the rate gives

$$\text{rate} = (0.681)(0.011)e^{-\frac{0.98}{k_B T}} [A][B]. \quad (9)$$

This equation is analogous to the general formula used to describe reaction kinetics in chemistry

$$\text{rate} = k(T)[A]^x[B]^y \quad (10)$$

where  $k(T)$  is the temperature dependent term and absorbed numerical pre-factors, and  $x, y$  are the order of the reaction for species  $A$  and  $B$  respectively.

## vi. Concentration dependence of the reaction rate II

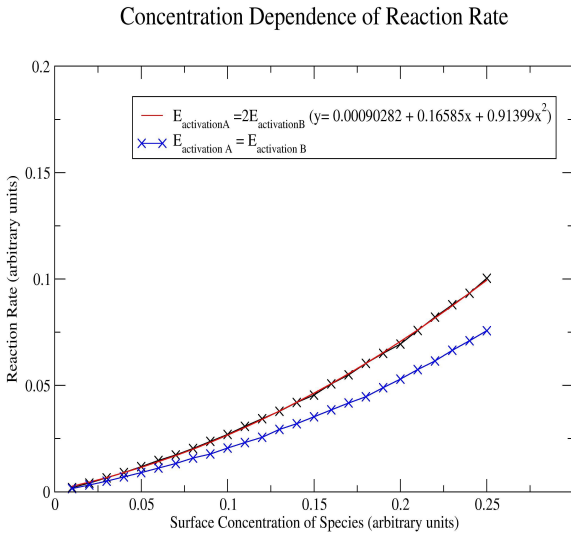


**Figure 7:** Concentration dependence of the reaction rate to calculate high  $T$  and low  $T$  activation energies for A-B reaction.  $\Delta E_A = 2\Delta E_B$  where the diffusion barrier for species B is lower relative to before ( $\Delta E_A = 1.0$  and  $\Delta E_B = 0.5$ ).

In figure 7, the overall quadratic fit of the curve remains the same, so the order of the reaction has not changed by changing diffusion barriers of  $A$  and  $B$  atoms. However, the rate has increased. This is because  $\Delta E_B$ , the energy barrier to diffusion for  $B$  atoms, was lowered, so more collisions occur.

## vii. Temperature dependence of the reaction rate II

In order to extract the high  $T$  and low  $T$  activation energy for the chemical reaction, it is assumed that the rate equation takes the form

$$R = a_A e^{-\frac{\Delta E_A}{k_B T}} + a_B e^{-\frac{\Delta E_B}{k_B T}} \quad (11)$$

where  $R$  is the rate,  $\Delta E_A$  and  $\Delta E_B$  are the energy barriers to diffusion for  $A$  and  $B$ , and  $a_A$  and  $a_B$  are constants.

**At low T,**  $k_B T \rightarrow 0$ . Therefore assume

$$e^{-\frac{\Delta E_A}{k_B T}} \ll a_B e^{-\frac{\Delta E_B}{k_B T}}, \quad (12)$$

so that equation 11 becomes

$$R = a_B e^{-\frac{\Delta E_B}{k_B T}}$$

which gives

$$\ln(R) = \ln(a_B) - \frac{\Delta E_B}{k_B T}. \quad (13)$$

**At high T,**  $1/k_B T \rightarrow 0$ . Using the Taylor expansion  $e^x \approx 1 + x$ ,

$$\begin{aligned} R &= a_A \left[ 1 - \frac{\Delta E_A}{k_B T} \right] + a_B \left[ 1 - \frac{\Delta E_B}{k_B T} \right] \\ &= (a_A + a_B) \left[ 1 - \frac{a_A \Delta E_A + a_B \Delta E_B}{(a_A + a_B) k_B T} \right] \end{aligned} \quad (14)$$

It follows that

$$\ln(R) = \ln(a_A + a_B) + \ln \left[ 1 - \frac{a_A \Delta E_A + a_B \Delta E_B}{(a_A + a_B) k_B T} \right] \quad (15)$$

Using  $\ln(1 + x) \approx x$ ,

$$\ln(R) = \ln(a_A + a_B) - \frac{a_A \Delta E_A + a_B \Delta E_B}{(a_A + a_B) k_B T}. \quad (16)$$

At low  $T$ , only the species with the lower activation energy ( $B$  in this case) is able to move, so the activation energy and rate of reaction is dependent on  $B$  diffusion alone. At high  $T$ , both species are able to hop, so the observed activation energy is a weighted average of their diffusion barriers.

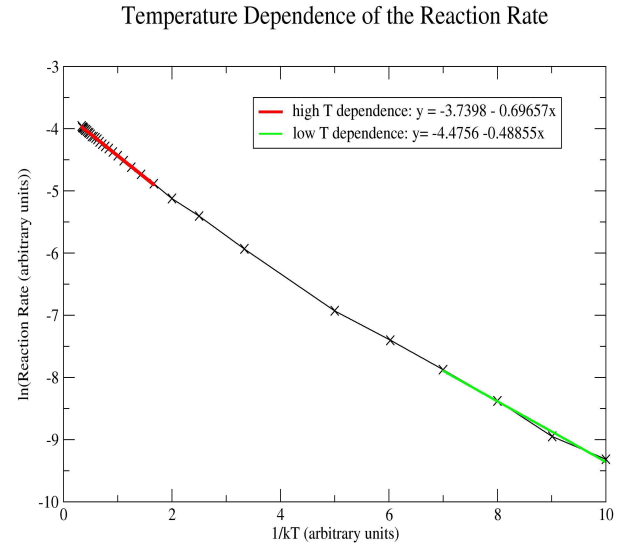


**Figure 8:** Temperature dependence of the reaction rate to find high and low  $T$  activation energies.

Using figure 8, the gradient at low  $T$  is 0.489. Comparing the fitted lines for low  $T$  and high  $T$  to equations 13 and 16 respectively gives;  $a_A = 0.012$ ,  $a_B = 0.011$ , and  $\Delta E_A = 0.93$ ,  $\Delta E_B = 0.49$ . These deviate from the input values ( $\Delta E_A = 1.0$ ,  $\Delta E_B = 0.5$ ) by 7% and 2% respectively. There is a higher deviation for the high  $T$  value: this is likely due to the fact that the atoms in the model no longer stay in such clearly defined potential wells, or that the calculation needs to be run to higher temperatures.

As expected overall,

$$R = 0.012 e^{-\frac{0.93}{k_B T}} + 0.011 e^{-\frac{0.49}{k_B T}}. \quad (17)$$

### III. OUTLOOK

Modelling complex systems with the kinetic Monte Carlo method is computationally slow and hard to write. The model also performs badly with a low concentration of adatoms, as seen in section [iii](#). However, the main limitation of kMC is that it relies on the external supply of information: such as rates and all possible reactions. For this reason, kMC is often combined with other methods in a broader multi-scale modelling approach.

For example, when investigating surface growth phenomena, DFT is used to find kinetic energy barriers for use in a kMC model. In dislocation dynamics in materials for fusion reactors, the dislocation motion is modelled by first inputting rates of kink nucleation and migration: calculated from transition state theory which approximates the rate constant<sup>3</sup>. kMC is also used to model vacancy diffusion in alloys (its original use), the viscoelasticity of crosslinked polymer networks, and clustering in ion or neutron irradiated solids.

### IV. SUMMARY AND CONCLUSION

In conclusion, a simple model of a catalytic surface reaction using kMC has been demonstrated in this project. It was shown that the diffusion coefficient is independent of time between measurements, and has an Arrhenius dependence on temperature. A coarse-grained continuum model showed that the reaction rate can be given as a function of temperature and concentration as follows:

$$\text{rate} = (0.681)(0.011)e^{-\frac{0.98}{k_B T}} [A][B].$$

Then the model was altered to study the effect of differing activation energies for diffusion for the species involved in the reaction. Similarly to before, the rate remained linear with respect to adatom concentration. The rate had a temperature dependence of:

$$\text{rate} = 0.012e^{-\frac{0.93}{k_B T}} + 0.011e^{-\frac{0.49}{k_B T}}.$$

Further useful investigation might include modelling a larger variation of activation energies, and non-diffusion limited reactions.

### REFERENCES

<sup>1</sup> Barber, Z. *Introduction to Materials Modelling*, Maney 2005., p. 106.

<sup>2</sup> Ibe, O. *Elements of Random Walk and Diffusion Processes*, John Wiley and Sons. 2013., p. 27.

<sup>3</sup> Voter, A. *Introduction to the Kinetic Monte Carlo Method*, in *Radiation Effects in Solids*, Springer 2005., p. 8.